Journal of Alloys and Compounds, 183 (1992) 241–251
JALCOM 7032

Structure and magnetic ordering of holmium carbide fluoride, Ho_2CF_2*

J. K. Cockcroft†, R. K. Kremer, Hj. Mattausch, N. P. Raju and A. Simon
Max-Planck-Institut für Festkörperforschung, Heisenbergstrasse 1, W-7000 Stuttgart 80 (FRG)

(Received July 1, 1991; accepted August 20, 1991)

Abstract

The preparation of a new rare earth carbide fluoride, Ho_2CF_2, is described. Ho_2CF_2 is trigonal, space group $P\bar{3}m1$, $Z=1$, with $a=3.6567(2)$ Å and $c=6.3171(5)$ Å at room temperature. On cooling below the Néel temperature of 3.7 K, Ho_2CF_2 transforms to an antiferromagnet with magnetic space group $P_a\bar{1}'$. The phase transition from the paramagnetic to antiferromagnetic state is accompanied by a distortion of the lattice to $P\bar{1}$ due to magnetoelastic effects. The nuclear and magnetic structures have been fully determined from high resolution powder neutron diffraction measurements at 1.5 and 50 K. Evidence for critical scattering above T_N is shown from specific heat, magnetic susceptibility and temperature-dependent neutron diffraction studies. Electrical conductivity measurements show that Ho_2CF_2 is an insulator. The relationship between the low dimensionality of the structure and the magnetic and physical properties of Ho_2CF_2 is discussed.

1. Introduction

The chemistry of the carbide halides of the rare earth elements is characterized by a large number of compounds, of which the gadolinium compounds have been extensively studied in closer detail [1] (see ref. 2 for a review of the chemical and physical properties of the metal-rich halides of the rare earths). In all the compounds synthesized so far, single carbon atoms or C_2 units are located in the octahedral voids formed by gadolinium metal atoms. These Gd_6C octahedral units may occur as isolated clusters or may be condensed to form extended arrays leading to chain and layer structures. In all the compounds the halogen atoms are coordinated to the edges of the Gd_6 octahedra.

So far, only one carbide fluoride has been synthesized, namely Gd_2CF_2 [3], in addition to the many chlorides, bromides and iodides. This paper reports on the preparation, crystal structure and magnetic and electrical properties of holmium carbide fluoride, Ho_2CF_2. The crystal structure is

*Dedicated to Professor W. Bronger and Professor Ch. J. Raub on the occasions of their 60th birthdays.

†Also at Institut Laue–Langevin, 156X, F-38042 Grenoble Cedex, France.

0925-8388/92/$5.00

largely characterized by the presence of extended bilayers and the highly anisotropic chemical bonding associated with them, implying interesting magnetic and electrical properties.

2. Experimental details

2.1. Sample preparation and characterization

The starting materials, holmium, HoF_3 and carbon, were prepared as follows. Sublimed holmium metal lumps (99.99%, Universal Matthey, Karlsruhe) were heated in a molybdenum crucible under hydrogen for 2 h at 900 K to produce holmium hydride. This was ground and then dehydrogenated at 1100 K for 5 h under high vacuum to yield powdered holmium metal. HoF_3 was prepared from Ho_2O_3 (99.99%, Universal Matthey) and HF following a method described by Greis and Petzel [4]. Carbon, in the form of activated charcoal (high purity, Merck, Darmstadt), was degassed at 1450 K in high vacuum for 24 h and stored in a pure argon atmosphere.

Of the rare earth carbide fluorides, the holmium derivative was thought to be easy to prepare owing to the fact that HoF_3 exhibits one of the lowest melting points of all the rare earth trifluorides. Ho_2CF_2 was synthesized from the starting materials holmium, HoF_3 and carbon in the molar ratio 4:2:3 (total mass approximately 2.5 g) sealed under 1 bar of argon in a tantalum ampoule, which was then sealed under vacuum in a quartz glass tube and heated to 1450 K for 8 days, resulting in the formation of a single-phase microcrystalline dark brown Ho_2CF_2 powder. Ho_2CF_2 slowly decomposes in air and is readily dissolved by dilute mineral acids at ambient temperature.

2.2. X-ray investigations

Powdered samples of Ho_2CF_2 were characterized at room temperature by the modified Guinier technique [5] with silicon ($a = 5.430\,35$ Å) as an internal standard using Cu $K\alpha_1$ ($\lambda = 1.540\,56$ Å). The diffraction patterns, which index as trigonal, matched those of the isostructural gadolinium compound Gd_2CF_2 [3] with space group $P\bar{3}m1$–D^3_{3d} (no. 164). The lattice constants, determined from coincidence measurements of 13 reflections in the range $4° < \theta < 30°$ ($\Delta\theta = \pm 0.005°$) refined [6] to $a = 3.6567(2)$ Å and $c = 6.3171(5)$ Å. The 20 largest d spacings (Å) are (with relative intensities) 6.317(10), 3.167(60), 2.831(100), 2.236(70), 2.106(5), 1.828(60), 1.754(50), 1.583(10), 1.582(40), 1.579(5), 1.536(30), 1.416(20), 1.413(10), 1.381(10), 1.266(20), 1.263(5), 1.197(10), 1.195(10), 1.176(40) and 1.119(20).

2.3. Specific heat

The specific heat was measured in an adiabatic calorimeter designed for the examination of small samples [7]. Powder samples with typical masses of about 500 mg were put in Duran glass ampoules and sealed under helium gas to ensure good thermal contact.

The magnetic contribution C_m to the heat capacity was obtained by subtracting a lattice contribution C_l which was estimated according to the

following procedure. A temperature-dependent Debye temperature $\Theta_D(T)$ was derived from the specific heat data $C_p(T)$ using (R, gas constant)

$$C_p = 9R\left(\frac{T}{\Theta_D}\right)^3 \int_0^{\Theta_D/T} \frac{e^x x^4}{(e^x - 1)^2}\, dx \tag{1}$$

At high temperature a polynomial was fitted to $\Theta_D(T)$. The polynomial was extrapolated to low temperatures and then used to calculate the lattice part of the heat capacity, C_l. The magnetic entropy S_m was calculated by numerically integrating C_m/T where C_m is the magnetic part of the heat capacity, $C_m = C_p - C_l$, following the thermodynamic relationship

$$S_m(T) = \int_0^T \frac{C_m(T')}{T'}\, dT' \tag{2}$$

2.4. Magnetic susceptibility

The susceptibility of powder samples (masses approximately 100 mg) was determined with a Quantum Design SQUID magnetometer. The samples were contained in dried gelatin capsules whose magnetizations were measured in separate runs and corrected for.

2.5. Electrical conductivity

The resistance was determined on an *in situ* pressed pellet employing a two-point electrometer method. The press was made from a Stennan cylinder and steel pistons and cooled in a continuous flow helium cryostat.

2.6. Neutron diffraction

For the neutron diffraction measurements, approximately 1 g of Ho_2CF_2 was sealed under helium gas in a thin-walled quartz glass ampoule 5 mm in diameter which was then supported in a thin-walled vanadium sample can 6 mm in diameter. Diffraction patterns were collected at the Institut Laue–Langevin, Grenoble on the high flux diffractometer D1B equipped with a 400-wire ^{3}He–Xe gas multidetector covering the 2θ range 15°–95°. The temperature was scanned at 0.05 °C min^{-1} over the range 1.5–7 K and the data were stored at approximately 60 s intervals (60 was chosen for obvious reasons). In addition, quick scans were taken between 7 and 300 K confirming the absence of further phase transitions in this temperature range. High resolution patterns of Ho_2CF_2 were collected on D1A at 1.5 and 50 K for the 2θ range 6°–156° in steps of 0.05° in about 20 and 23 h respectively.

3. Results and discussion

The structure of Ho_2CF_2 was refined in the trigonal space group $P\bar{3}m1$ by the Rietveld method [8] using the program PROFIL [9] from the

D1A data collected on the sample at 50 K. From the 2900 data points containing 48 contributing reflections, a total of 13 parameters (of which six are structural) were refined. The final parameters, which are uncorrected for the effects of absorption, are shown in Table 1, with the best fit to the data displayed in Fig. 1. The correction to the temperature factors due to the effect of absorption is estimated at about 0.2 Å^2.

Figure 2 shows a projection of the structure along [110]. The structure may be described in terms of Ho_6 octahedra filled with carbon atoms which are connected via their edges to form infinite $[Ho_2C]$ layers. The coordination of the remaining edges by fluorine atoms results in $[Ho_2C]$ layers sandwiched between fluorine layers and stacked along [001] according to the sequence $\cdots$AbγaB$\cdots$ ($\cdots$FHoCHoF$\cdots$). Such FHoCHoF layers are held together by van der Waals forces. Owing to the trigonal symmetry, only two short metal–metal distances are found: the shortest (3.41 Å) is between the planes of the metal bilayers and the second, within the plane, is equal to the lattice constant a (3.65 Å).

The structure type is well known from a great number of different compounds such as Gd_2Br_2C [10], $CaAl_2Si_2$ [11], Ta_2S_2C [12], Ce_2O_2S [13] and Ln_2O_3 [14], which have structural subunits $[CGd_2]$, $[CaSi_2]$, $[CTa_2]$, $[SCe_2]$ and $[OLn_2]$ respectively based on the CdI_2 structure [15]. The remaining atoms fill the tetrahedral holes between the metal or silicon double layers.

Conductivity experiments show that Ho_2CF_2 is non-metallic as predicted by the simple ionic description $(Ho^{3+})_2C^{4-}(F^-)_2$. The resistance of the measured pellet is of the order of several megaohms at room temperature and increases by three orders of magnitude on cooling to liquid helium temperature. The result is similar to that observed for the layered metal-rich rare earth halides in which all voids in the metal atom bilayer are fully

TABLE 1

Final parameters, R factors and interionic distances for Ho_2CF_2 at 50 K. R factors are defined as in ref. 8 with y_i(obs) referring only to the Bragg intensity, *i.e.* y_i(obs)=y_i(total) − y_i(background). Weights are given by $1/\sigma_{y(\text{obs})}{}^2$. Scattering lengths Ho=8.37 fm, C=5.65 fm, F=6.65 fm [22]. λ=1.911 Å. Space group $P\bar{3}m1$. a=3.653 73(1) Å, c=6.3098(2) Å. V=72.949(2) Å^3, ρ_{calc}=8.646 g cm^{-3}

Atom	Site	symmetry	X	Y	Z	B (Å^2)	N
Ho	2d	$3m$	$\frac{1}{3}$	$\frac{2}{3}$	0.7876(6)	−0.16(7)	2
C	1a	$\bar{3}m$	0	0	0	0.07(14)	1
F	2d	$3m$	$\frac{1}{3}$	$\frac{2}{3}$	0.3882(6)	0.51(10)	2

U, V, W (deg^2): 0.172(5), −0.423(13), 0.365(7)

R_{wp}=6.3%, R_{exp}=3.6%, R_I=3.8%

Interatomic distances (Å)

Ho–Ho	3.411(4), 3.653(1)	Ho–C	2.499(2)	Ho–F	2.520(5), 2.383(3)
F–F	2.538(3)	F–C	3.233(3)		

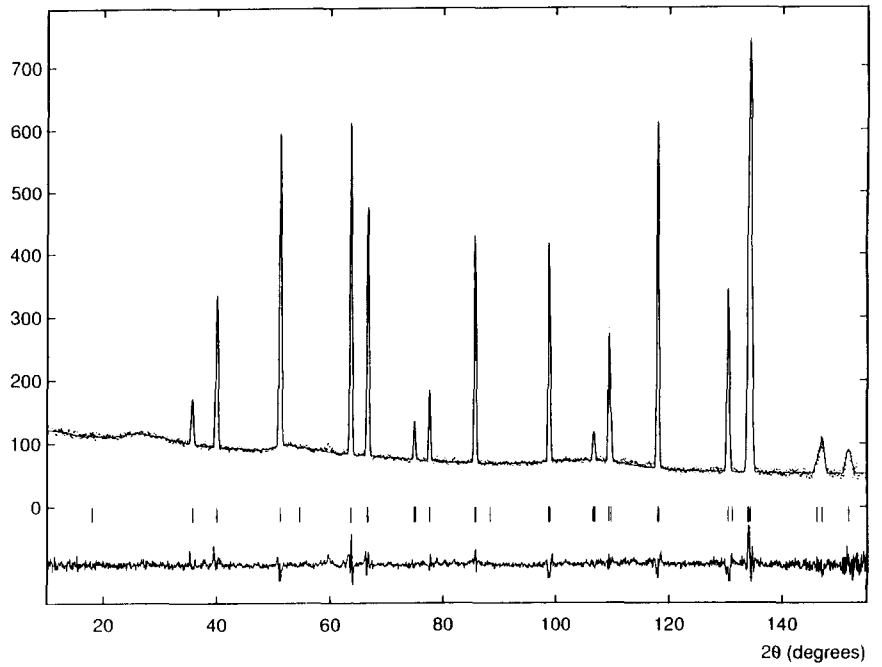

Fig. 1. Observed, calculated and difference profiles for Ho_2CF_2 at 50 K measured on D1A with $\lambda = 1.911$ Å. Vertical tick marks indicate calculated reflection positions. The background, estimated by graphical methods, has a large contribution from paramagnetic scattering which decreases as the holmium form factor with increasing scattering angle. The broad maxima in the background are due to diffuse scattering from the quartz ampoule.

filled with hydrogen interstitials, *e.g.* $RE^{3+}X^{-}(H^{-})_2$ [1, 2], in contrast to the rare earth halide dicarbides which from the C–C bond length are best formulated as $(RE^{3+})_2(C^{4-})_2(X^{-})_2$ [16]. The latter are metallic owing to covalent interaction of the occupied C–C π orbitals with empty metal d states.

The specific heat (Fig. 3) shows a large anomaly with a singularity at 3.61(5) K and a long tail towards higher temperatures with large contributions up to 25 K. The specific heat indicates a phase transition which is shown to be of antiferromagnetic origin from the magnetic susceptibility measurements (Fig. 4). The latter exhibit a maximum at 4.6 K and a steep decrease below. The derivative $d(\chi T)/dT$ (*Fisher's heat capacity* [17]) shows a peak at 3.7(1) K in agreement with the specific heat data. The high temperature susceptibility follows a Curie–Weiss law

$$\chi_{mol} = \frac{C}{T - \Theta} \tag{3}$$

with a paramagnetic Curie temperature Θ equal to $-4.9(2)$ K, indicating predominantly antiferromagnetic exchange interactions. The Curie constant

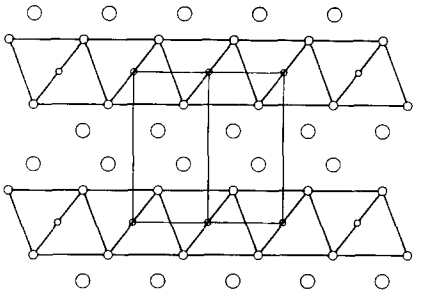

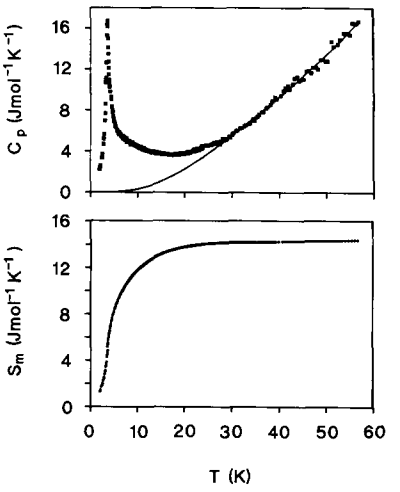

Fig. 2. Projection of the structure as seen down [110]. Holmium, carbon and fluorine are represented by medium, small and large circles respectively.

Fig. 3. (a) Specific heat C_p and estimated lattice heat capacity C_l (full curve) of Ho_2CF_2. (b) Magnetic part S_m of the entropy according to eqn. (2). (All data are per one formula unit of $HoC_{0.5}F$.)

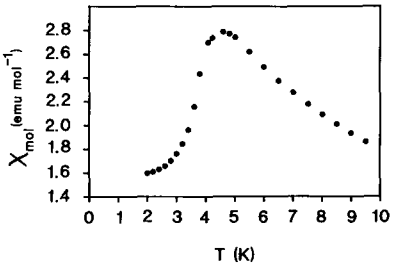

Fig. 4. Molar magnetic susceptibility χ_{mol} of Ho_2CF_2 at low temperatures.

C corresponds to an effective magnetic moment of 9.4 μ_B, which is slightly lower than the expected free-ion value of 10.6 μ_B.

From the diffraction patterns collected on D1B (Fig. 5) it is evident that between 1.5 K and room temperature Ho_2CF_2 exhibits only one phase transition at about 4 K, in agreement with the specific heat (Fig. 3) and magnetic susceptibility (Fig. 4) measurements. The extra peaks that appear at low temperature in Fig. 5 are attributed to antiferromagnetic ordering of the magnetic spins of the Ho^{3+} ions and may be indexed in terms of a doubling of the trigonal unit cell along a with consequent loss of threefold symmetry. Several magnetic space groups are possible and the correct structure was determined by trial and error to have the magnetic space group symmetry $P_a\bar{1}'$.

The complete magnetic structure was refined by the Rietveld method from the D1A data of Ho_2CF_2 at 1.5 K (Fig. 6) using the program MPROF

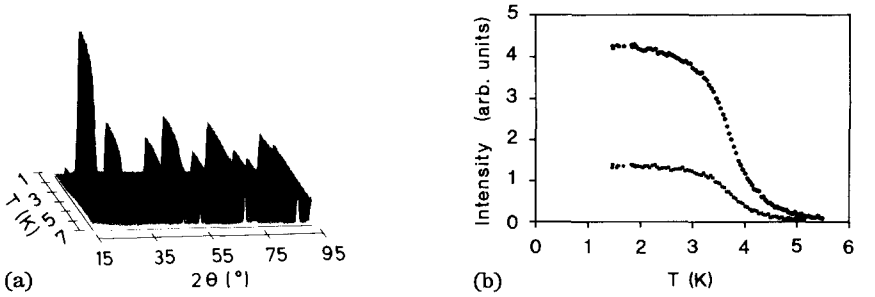

Fig. 5. (a) Diffraction patterns of Ho_2CF_2 as a function of temperature between 1.5 and 7 K obtained on heating on D1B with $\lambda = 2.52$ Å. The small feature at about 20° is an experimental artefact due to a bad wire of the multidetector. (b) Intensity of the two strongest magnetic reflections $\frac{1}{2}00$ (upper) and $\frac{1}{2}01 + \frac{1}{2}0\bar{1}$ (lower) between 1.5 and 7 K.

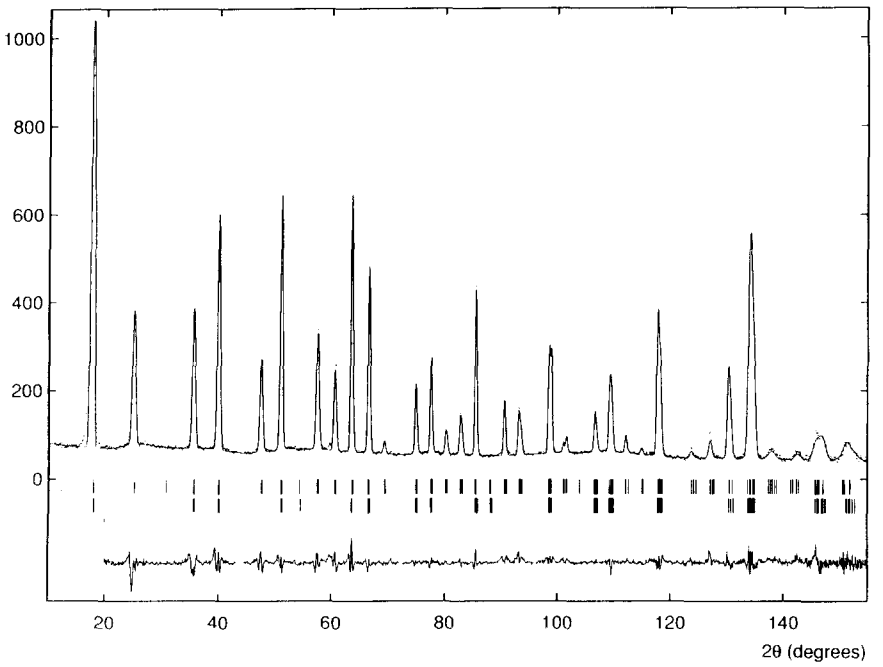

Fig. 6. Observed, calculated and difference profiles for Ho_2CF_2 at 1.5 K measured on D1A with $\lambda = 1.911$ Å. Upper and lower vertical tick marks indicate calculated positions of magnetic and nuclear reflections respectively. Horizontal bar shows region of pattern excluded from Rietveld least-squares refinement. Relative to the diffraction pattern of Ho_2CF_2 at 50 K, the background is considerably reduced owing to loss of the paramagnetic scattering below T_N.

[18] with the reflection condition hkl, $h = n + \frac{1}{2}$ and with $a \approx b$, $\alpha \approx \beta \approx 90°$ and $\gamma \approx 120°$. The magnetic form factor for Ho^{3+} was taken from tables by Brown [19]. During the initial refinements the trigonal symmetry conditions for the cell constants were maintained ($a = b$, $\alpha = \beta = 90°$, $\gamma = 120°$) and the refinement converged to $R_{wp} = 17.1\%$ with $R_{exp} = 5.6\%$. Closer examination

of the D1A data shows that the nuclear peaks are split at high angle and this is readily seen for the peak at 98.7° in Fig. 6 where the diffractometer has its best resolution. Removal of the symmetry conditions applied to the cell constants gave a significantly better fit to the data with $R_{wp} = 11.4\%$. However, it was apparent from the difference profile that the magnetic peaks were slightly broadened with respect to the nuclear peaks and a multiphase fit to the data was carried out with separate U, V and W parameters to describe the peak widths as a function of 2θ for the nuclear and magnetic peaks. The best fit to the data, shown in Fig. 6, with $R_{wp} = 9.0\%$, was achieved with 23 parameters (of which nine are structural) in which the x, y coordinates of Ho and F were fixed at 0.6667, 0.3333 as in the trigonal structure and with the intense magnetic peak at 17.9° excluded from the refinement owing to instrumental asymmetry effects. The final parameters and R factors are listed in Table 2.

The arrangement of the magnetic moments corresponds to an antiferromagnetic collinear structure with the propagation vector along [100]. In the ab plane the components of the magnetic moments lie 17° off the [010] direction and are tilted out of the ab plane by 24° as illustrated in Fig. 7. The total magnetic moment refined to 7.63(5) μ_B.

An interesting result of the high resolution D1A data analysis is the observation of lattice deformation due to magnetoelastic effects. The magnitude of this distortion is very small and is generally not observable in the low resolution diffraction patterns commonly used to determine magnetic structures on D1B. The difference between the a and b lattice constants is of the order of 0.02% and the angles deviate from those of the trigonal lattice by only 0.2%. The reduction in symmetry from $P\bar{3}m1$ to $P\bar{1}$ on transforming to the low temperature antiferromagnetic phase is consistent in terms of subgroup–supergroup relationships with the observation of the colour space

TABLE 2

Final parameters and R factors for Ho_2CF_2 at 1.5 K. $\lambda = 1.911$ Å. Nuclear space group $Pa\bar{1}$, magnetic space group $P_a\bar{1}'$. $a = 3.6517(2)$ Å, $b = 3.6510(2)$ Å, $c = 6.3085(2)$ Å, $\alpha = 90.121(5)°$, $\beta = 89.808(3)°$, $\lambda = 119.893(3)°$. $V = 72.918(4)$ Å^3, $\rho_{calc} = 8.642$ g cm^{-3}

Atom	Site	symmetry	X	Y	Z	B (Å^2)	N
Ho	2i	1	0.6667	0.3333	0.7859(6)	−0.14(5)	2
C	1a	$\bar{1}$	0	0	0	−0.01(10)	1
F	2i	1	0.6667	0.3333	0.3858(6)	0.36(9)	2

M (μ_B): 7.63(5)
k_x, k_y, k_z (μ_B): −2.34(13), 5.46(6), 3.19(9)
U, V, W (deg^2) (nuclear): 0.17(1), −0.37(2), 0.33(1)
U, V, W (deg^2) (magnetic): 0.38(2), −0.87(3), 0.65(1)
$R_{wp} = 9.0\%$, $R_{exp} = 6.4\%$, $R_I = 4.4\%$, R_I(nuclear) = 2.0%, R_I(magnetic) = 7.5%

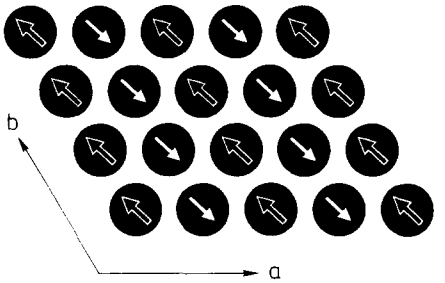

Fig. 7. View of the magnetic structure as seen in the *ab* plane (single holmium layer only). Black and white arrows indicate magnetic moments tilted above and below the plane respectively.

group $P_a\bar{1}'$ for the magnetic structure. Although the high resolution patterns are only available for 1.5 and 50 K, it is reasonable to assume that the onset of lattice distortion is directly coupled via magnetoelastic interactions to the onset of long-range antiferromagnetic ordering. Such a behaviour is not uncommon for rare earth compounds [20] although it is not often observed.

At 1.5 K the difference in peak widths between magnetic and nuclear reflections is attributed to a shorter coherence length for the magnetic structure. This is not so surprising given that Ho_2CF_2 is a layered structure with very anisotropic magnetic interactions. Evidence for the latter is further shown in the analysis of the intensities of the magnetic Bragg reflections measured on D1B as a function of temperature (Fig. 5). The sigmoidal-shaped curve demonstrates the existence of significant critical scattering due to short-range magnetic ordering within the layers. This interpretation is also corroborated by the broad maximum above T_N in the magnetic susceptibility and the high temperature tail in the specific heat, both of which are indicative of magnetic short-range ordering. About two-thirds of the total magnetic entropy occurs above T_N (Fig. 3).

The temperature dependence of the intensities of the magnetic Bragg reflections obtained from the D1B experiment shows a point of inflection around 3.7(1) K in good agreement with the critical temperature deduced from specific heat and susceptibility measurements. The order of magnitude of T_N observed for Ho_2CF_2 is comparable to that detected for other insulating layered metal-rich rare earth halides containing hydrogen as the interstitial atoms, *e.g.* $REXH_2$ (RE≡Gd, Tb; X≡Cl, Br, I) [1, 2], whereas the ordering temperatures for metallic layered dicarbides, *e.g.* $RE_2C_2Br_2$ (RE≡Gd, Tb) are about one order of magnitude larger [16]. The absence of conduction electrons excludes RKKY interactions and leaves superexchange and long-range dipolar coupling via the anions as the only source of interaction between the Ho^{3+} magnetic moments. Since the 4f electrons are little involved in chemical bonding, the superexchange mechanism is typically small and dipolar interactions are of equal importance. Given that interlayer coupling cannot be neglected, Ho_2CF_2 is not an ideal two-dimensional magnetic system.

Owing to crystal field effects, the magnitude of the holmium magnetic moment is lower than the maximum possible moment of 10 μ_B expected

for the $^5I_8$ ground term (Landé factor $g_J=\frac{5}{4}$) of Ho^{3+} with $4f^{10}$ electronic configuration. In Ho_2CF_2 the degeneracy of the ground term is lifted by a crystal electric field of C_{3v} symmetry, in principle allowing that Ho_2CF_2 could *a priori* be diamagnetic at low temperatures, with a singlet as the crystal field ground state, which obviously is not the case for Ho_2CF_2. The magnetic entropy is found to be 14.4 J mol^{-1} K^{-1} or $R\times 1.73$, being close to $R\ln 6$ (Fig. 3), and indicates the ordering of a six-level system. Such a large degeneracy for the crystal field ground state, on the other hand, seems unlikely in view of the low site symmetry. We suggest that a substantial part of the entropy also originates from the structural phase transition.

Assuming as a first approximation that the magnetic ordering takes place in a crystal field doublet as, for example, was observed for $Ho(OH)_3$ [21], ground state eigenfunctions composed primarily of $J_z=\pm 6$ states could account for the experimentally detected magnetic moment of 7.63 μ_B. Inelastic neutron-scattering experiments should be carried out to establish the full crystal field level scheme of Ho^{3+} in Ho_2CF_2 in order to enable a detailed comparison with the results reported here.

Acknowledgments

We thank E. Brücher, H. Diem, R. Eger and W. Röthenbach for experimental help and E. Gmelin for very valuable discussions. N.P.R. gratefully acknowledges full financial support by the DAAD (German Academic Exchange Service).

References

1 A. Simon, *J. Solid State Chem.*, *57* (1986) 2;
Hj. Mattausch, C. Schwarz and A. Simon, *Z. Kristallogr.*, *178* (1987) 156;
C. Bauhofer, Hj. Mattausch, G. J. Miller, W. Bauhofer and A. Simon, *J. Less-Common Met.*, *167* (1990) 65.
2 A. Simon, Hj. Mattausch, G. J. Miller, W. Bauhofer and R. K. Kremer, in K. A. Gschneidner Jr. and L. Eyring (eds.), *Handbook on the Physics and Chemistry of Rare Earths*, Vol. 15, North-Holland, Amsterdam, 1991, p. 191.
3 Hj. Mattausch, R. Eger and A. Simon, *Z. anorg. allg. Chem.*, *597* (1991) 145.
4 O. Greis and T. Petzel, *Z. anorg. allg. Chem.*, *403* (1974) 1.
5 A. Simon, *J. Appl. Crystallogr.*, *3* (1970) 1.
6 K. F. Tebbe, Program AGL, *Ph.D. Thesis*, Universität Münster, 1970.
7 E. Gmelin and K. Ripka, *Cryogenics*, *21* (1981) 177.
8 H. M. Rietveld, *J. Appl. Crystallogr.*, *2* (1969) 65.
9 J. K. Cockcroft, Program PROFIL V4.05: a Rietveld program for the refinement of crystal structures from single and multiphase powder neutron and synchrotron radiation data, Institut Laue-Langevin, Grenoble, 1991.
10 U. Schwanitz-Schüller and A. Simon, *Z. Naturf. B*, *40* (1985) 710.
11 E. I. Gladyshevskii, P. I. Krypyakevich and O. I. Bodak, *Ukr. Fiz. Zh.*, *12* (1967) 454.
12 O. Beckmann, H. Boller and H. Nowotny, *Monatsh. Chem.*, *101* (1970) 945.
13 W. H. Zachariasen, *Acta Crystallogr.*, *2* (1949) 60.
14 P. Adelbert and J. P. Traverse, *Mater. Res. Bull.*, *14* (1979) 303.

15 Z. G. Pinsker, *Zh. Fis. Khim.*, *15* (1941) 559.
16 Hj. Mattausch, R. Eger, R. K. Kremer and A. Simon, *Z. anorg. allg. Chem.*, in the press.
17 M. E. Fisher, *Proc. R. Soc. (Lond.) A*, *254* (1960) 66; *Philos. Mag.*, *7* (1962) 1731.
18 M. W. Thomas and P. J. Bendall, *Acta Crystallogr. A*, *34* (1978) S351.
19 P. J. Brown, personal communication, 1991.
20 F. Lèvy, *Phys. Kondens. Mater.*, *10* (1969) 71.
M. E. Mullen, B. Lüthi, P. S. Wang, E. Bucher, L. D. Longinotti and J. P. Maita, *Phys. Rev. B*, *10* (1974) 186.
21 C. A. Catanese and H. E. Meissner, *Phys. Rev. B*, *8* (1973) 2060.
22 L. Koester and H. Rauch, Recommended values on neutron scattering lengths, *IAEA Rep. 2517/RB*, 1983 (International Atomic Energy Agency, Vienna).